Quantum-Enhanced Optical-Phase Tracking

Hidehiro Yonezawa *et al.*

Science **337**, 1514 (2012);
DOI: 10.1126/science.1225258

demonstrates that circumbinary planets can exist in habitable zones. Although the definition of the habitable zone assumes a terrestrial planet atmosphere, which does not apply for Kepler-47 c, large moons, if present, would be interesting worlds to investigate.

A 0.2% deep transit-like event is present at time 2,455,977.363 (BJD, barycentric Julian date) that is not caused by either of the two planets. A search for additional transits has revealed several more tentative transit events (*12*), but we caution that the star is faint (the Kepler magnitude is 15.178), there are large modulations due to star-spots, and the data contain correlated "red" noise, making small, nonperiodic transit detection challenging. The marginal evidence at present is insufficient to place confidence on any additional candidate planet(s).

The primary star is similar to the Sun in both mass and radius, and dominates the luminosity of the binary system, having 60 times the bolometric luminosity of the secondary star (or 176 times the brightness in the Kepler bandpass). A spectroscopic analysis gives an effective temperature of 5636 ± 100 K for the primary star (table S2), with a metallicity slightly less than solar ([M/H] = −0.25 ± 0.08 dex). The star's rotation period as determined from the star-spot modulation in the light curve (*12*) is only 4% longer than the orbital period, suggesting that the spin and orbital angular momenta have been synchronized by tidal interactions. Supporting this interpretation, the obliquity of the primary star (the angle between the spin and orbital axes) must be smaller than about 20°, based on the observable effects of the secondary star eclipsing star-spots on the primary star (*12*, *18*–*21*). Star-spot crossings also perturb the shape and depth of the primary eclipses, leading to systematic trends in the eclipse times, and limit the precision with which one can infer the planets' masses. In addition, the loss of light due to star-spots causes eclipses to appear slightly deeper than they would for an unspotted star, biasing the determination of the stellar and planetary radii too high by a few percent.

With Kepler-47 b and c, six confirmed transiting circumbinary planets are currently known. Their orbital periods relative to their host binary stars show no tendency to be in resonance, and their radii are Saturn-size and smaller. Given that Jupiter-size planets are easier to detect, their absence in the Kepler data suggests that the formation and migration history of circumbinary planets may disfavor Jupiter-mass planets orbiting close to the stars, in accord with (*22*).

The planets in Kepler-47 are expected to have formed much farther out than their present orbits, at locations where the conditions for the formation of giant planets are more favorable (*9*, *10*). The planets have likely migrated to their current orbits as a result of interactions with the circumbinary disk. The multiplicity and coplanarity of the orbits strengthen the argument for a single-disk formation and a migration scenario for circumbinary planetary systems. However, unlike orbits around a single star, the environment around a binary star is much more dynamic and tends to augment planet-planet interactions. The relatively large distance between the orbits of the inner and outer planets in the Kepler-47 system is consistent with requirements for dynamical stability (*23*).

The previously detected transiting circumbinary planet systems show no evidence for more than a single planet. The multiplanet nature of the Kepler-47 system establishes that despite the chaotic environment around binary stars, planetary systems can form and persist close to the binary, and invites a broader investigation into how circumbinary planets compare to planets and planetary systems around single stars.

References and Notes

1. D. G. Koch *et al.*, *Astrophys. J.* **713**, L79 (2010).
2. W. J. Borucki *et al.*, *Science* **327**, 977 (2010).
3. N. M. Batalha *et al.*, *Astron. J.* **141**, 83 (2011).
4. R. W. Slawson *et al.*, *Astron. J.* **142**, 160 (2011).
5. L. R. Doyle *et al.*, *Science* **333**, 1602 (2011).
6. W. F. Welsh *et al.*, *Nature* **481**, 475 (2012).
7. J. A. Orosz *et al.*, http://arxiv.org/abs/1208.3712 (2012).
8. S. Meschiari, *Astrophys. J.* **752**, 71 (2012).
9. S.-J. Paardekooper *et al.*, *Astrophys. J.* **754**, L16 (2012).
10. T. Borkovits *et al.*, *Astron. Astrophys.* **398**, 1091 (2003).
11. See the supplementary materials on *Science* Online.
12. J. A. Carter *et al.*, *Science* **331**, 562 (2011).
13. S. R. Kane, D. M. Gelino, *Publ. Astron. Soc. Pac.* **124**, 323 (2012).
14. J. J. Lissauer *et al.*, *Astrophys. J. Suppl. Ser.* **197**, 8 (2011).
15. M. J. Holman, P. A. Wiegert, *Astron. J.* **117**, 621 (1999).
16. J. F. Kasting *et al.*, *Icarus* **101**, 108 (1993).
17. R. Sanchis-Ojeda *et al.*, *Astrophys. J.* **733**, 127 (2011).
18. P. A. Nutzman *et al.*, *Astrophys. J.* **740**, L10 (2011).
19. J. M. Désert *et al.*, *Astrophys. J. Suppl. Ser.* **197**, 14 (2011).
20. R. Sanchis-Ojeda *et al.*, *Nature* **487**, 449 (2012).
21. A. Pierens, R. P. Nelson, *Astron. Astrophys.* **483**, 633 (2008).
22. A. N. Youdin *et al.*, *Astrophys. J.* **755**, 17 (2012).
23. D. R. Underwood *et al.*, *Int. J. Astrobiol.* **2**, 289 (2003).

Acknowledgments: Kepler was selected as the 10th mission of the Discovery Program. Funding for this mission is provided by NASA, Science Mission Directorate. The Kepler data presented in this paper were obtained from the Mikulski Archive for Space Telescopes (MAST). The Space Telescope Science Institute (STScI) is operated by the Association of Universities for Research in Astronomy, Inc., under NASA contract NAS5-26555. Support for MAST for non-HTS data is provided by the NASA Office of Space Science via grant NXX09AF08G and by other grants and contracts. This work is based in part on observations obtained with the Hobby-Eberly Telescope, which is a joint project of the University of Texas at Austin, the Pennsylvania State University, Stanford University, Ludwig-Maximilians-Universität München, and Georg-August-Universität Göttingen. J.A.O. and W.F.W. acknowledge support from the Kepler Participating Scientist Program via NASA grant NNX12AD23G; J.A.O., W.F.W., and G.W. also gratefully acknowledge support from the NSF via grant AST-1109928. G.T. acknowledges partial support for this work from NSF grant AST-1007992. J.A.C. and D.C.F. acknowledge NASA support through Hubble Fellowship grants HF-51267.01-A and HF-51272.01-A, respectively, awarded by STScI. Our dear friend and colleague David G. Koch passed away after this work was completed. He was a critical part of Kepler's success, and he will be missed.

Supplementary Materials

www.sciencemag.org/cgi/content/full/science.1228380/DC1
Materials and Methods
Supplementary Text
Figs. S1 to S25
Tables S1 to S9
References (*25*–*59*)

3 August 2012; accepted 22 August 2012
Published online 28 August 2012;
10.1126/science.1228380

Quantum-Enhanced Optical-Phase Tracking

Hidehiro Yonezawa,[1] Daisuke Nakane,[1] Trevor A. Wheatley,[1,2,3] Kohjiro Iwasawa,[1] Shuntaro Takeda,[1] Hajime Arao,[1] Kentaro Ohki,[4] Koji Tsumura,[5] Dominic W. Berry,[6,7] Timothy C. Ralph,[2,8] Howard M. Wiseman,[9]* Elanor H. Huntington,[2,3] Akira Furusawa[1]*

Tracking a randomly varying optical phase is a key task in metrology, with applications in optical communication. The best precision for optical-phase tracking has until now been limited by the quantum vacuum fluctuations of coherent light. Here, we surpass this coherent-state limit by using a continuous-wave beam in a phase-squeezed quantum state. Unlike in previous squeezing-enhanced metrology, restricted to phases with very small variation, the best tracking precision (for a fixed light intensity) is achieved for a finite degree of squeezing because of Heisenberg's uncertainty principle. By optimizing the squeezing, we track the phase with a mean square error 15 ± 4% below the coherent-state limit.

There are many tasks where precise optical phase estimation is critical, including communication (*1*, *2*) and metrology (*3*). Quantum mechanics imposes a fundamental bound on precision (*4*–*6*), and this already limits gravitational wave detection (*7*–*9*) and can guarantee security in quantum cryptography (*10*). The quantum limits are determined by optimizing (subject to constraints) the input quantum state, the quantum measurement, and the data processing. Much effort has been devoted to approaching the fundamental quantum limits (*3*, *5*, *6*).

Phase estimation can be divided into two kinds (*11*): phase sensing, where the phase is known to always lie within some small interval [e.g., (*12*)], and general phase estimation, where

it is not so constrained [e.g., (*11*)]. In the former case, when (as in most practical situations) the field has a large coherent amplitude, the problem can be linearized in terms of the phase rotation (*7*), which greatly simplifies the task of optimizing the input state and the measurement. By contrast, in the case of unconstrained phase estimation the problem cannot be linearized, and as a consequence the optimization problem is considerably harder (*11*, *13*–*22*). Although a quantum enhancement of phase sensing using nonclassical states of light has recently been demonstrated (*8*, *9*), this has been done for general phase estimation only with postselected results (*11*).

We present a demonstration of unconstrained phase estimation with a quantum enhancement using nonclassical (squeezed) states. We used homodyne detection, with no postselection of data and no compensation for losses or detector inefficiency in the system. Moreover, the problem of a stochastically varying phase is addressed (*8*, *9*, *19*–*22*), as is highly relevant for physical metrology and communication, rather than a time-invariant (but initially unknown) phase (*11*–*13*, *15*–*18*). To perform optimal estimation, we have implemented optical-phase tracking: a phase-lock loop that strives to maintain the maximum measurement sensitivity for a widely varying phase. The quantum noise in the photocurrent prevents the maximum sensitivity from being perfectly maintained, which is why we observe an optimal degree of squeezing.

Our experiment (Fig. 1A) used a continuous-wave optical phase–squeezed beam. The phase of the beam is modulated with the signal $\varphi(t)$, the waveform to be estimated (*22*–*24*). As in (*21*, *22*), we used a stochastic waveform defined by

$$\varphi(t) = \sqrt{\kappa}\int_{-\infty}^{t} e^{-\lambda(t-s)}dV(s) \qquad (1)$$

Here, $dV(s)$ is a classically generated Wiener process (*25*) (white noise), λ^{-1} is the correlation time of $\varphi(t)$, and κ determines the magnitude of the phase variation, which is of order unity. This $\varphi(t)$ is a continuous-time random walk with a tendency to return to the mean phase of zero, a kind of noisy relaxation process that occurs in many physical situations (*25*).

The phase-modulated beam was measured by homodyne detection, using a local oscillator (LO) and yielding a noisy current $I(t)$. The LO phase $\Phi(t)$ was feedback-controlled to be $\Phi(t) \approx \pi/2 + \varphi(t)$, because this is the most sensitive operating point for sensing changes in $\varphi(t)$ (Fig. 1B). Because $\varphi(t)$ is unknown, the best strategy is adaptive metrology (*11*, *13*, *15*–*21*), in which feedback control is used to set $\Phi(t) = \varphi_f(t) + \pi/2$, where $\varphi_f(t)$ is a filtered estimate of $\varphi(t)$, that is, an estimate based on $I(s)$ for all $s < t$. This gives a normalized homodyne output current $I(t)$ of (*19*, *26*),

$$I(t)dt \simeq 2|\alpha|[\varphi(t) - \varphi_f(t)]dt + \sqrt{\overline{R}_{sq}}dW(t)$$

$$\overline{R}_{sq} = \sigma_f^2 e^{2r_p} + (1-\sigma_f^2)e^{-2r_m} \qquad (2)$$

Here, $|\alpha|$ is the amplitude of the input phase-squeezed beam, and $dW(t)$ is another Wiener process (*25*) arising from the squeezed vacuum fluctuations. The magnitude $\overline{R}_{sq}$ of these quantum fluctuations is determined by the degree of squeezing ($r_m \geq 0$) and antisqueezing ($r_p \geq r_m$) and by $\sigma_f^2 = \langle[\varphi(t) - \varphi_f(t)]^2\rangle$. Note that several approximations, justified in (*26*), have been made to derive Eq. 2, most notably a second-order expansion for $I(t)dt$ in the small variable $[\varphi(t) - \varphi_f(t)]$.

For optimal feedback control, the Kalman filter was used for $\varphi_f(t)$ (*22*), which is the causal (i.e., real time) estimator with the lowest mean square error (MSE). The Kalman filter is the optimal filter for estimating $\varphi(t)$ of the form of Eq. 1 when using a coherent beam (*22*), and the calculation generalizes to our squeezed case (*26*). Although the filtered estimate $\varphi_f(t)$ is a good estimate of the signal phase $\varphi(t)$, to obtain the best estimate we applied the acausal technique of smoothing (*21*, *22*, *24*). After storing data over a certain period of time, a precise estimate of $\varphi_s(t)$ was obtained at a time t in the middle of that period by using observations both before and after t. The MSE of the smoothed estimate $\sigma_s^2 = \langle[\varphi(t) - \varphi_s(t)]^2\rangle$ is given as (*22*, *26*),

$$\sigma_s^2 = \kappa \Big/ \left(2\sqrt{4\kappa|\alpha|^2 / \overline{R}_{sq} + \lambda^2}\right) \qquad (3)$$

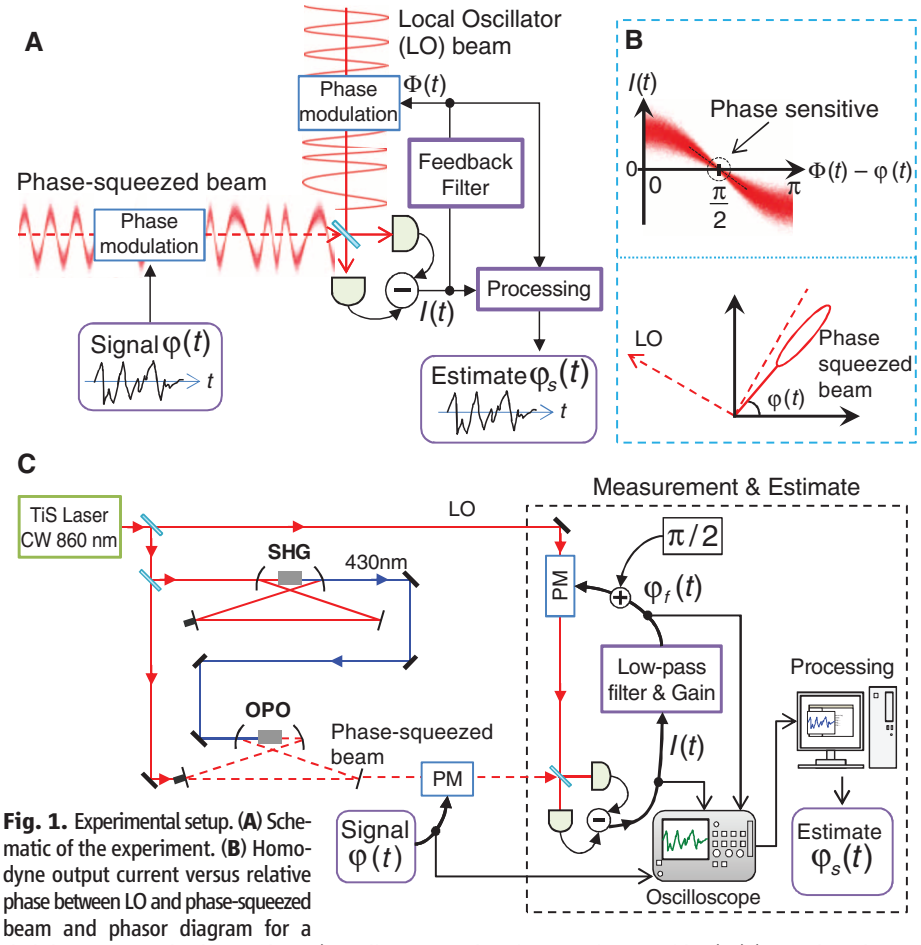

Fig. 1. Experimental setup. (**A**) Schematic of the experiment. (**B**) Homodyne output current versus relative phase between LO and phase-squeezed beam and phasor diagram for a slightly nonoptimal relative phase (as will occur in the phase-tracking problem). (**C**) Detail of the experimental setup. The abbreviations are TiS, titanium sapphire; CW, continuous-wave; PM, phase modulator; and SHG, second-harmonic-generation.

[1]Department of Applied Physics, School of Engineering, The University of Tokyo, 7-3-1 Hongo, Bunkyo-ku, Tokyo 113-8656, Japan. [2]Centre for Quantum Computation and Communication Technology, Australian Research Council, Canberra, Australia. [3]School of Engineering and Information Technology, University College, The University of New South Wales, Canberra, ACT 2600, Australia. [4]Department of Applied Mathematics and Physics, Graduate School of Informatics, Kyoto University, Yoshida-Honmachi, Sakyo-ku, Kyoto 606-8501, Japan. [5]Department of Information Physics and Computing, The University of Tokyo, 7-3-1 Hongo, Bunkyo-ku, Tokyo 113-0033, Japan. [6]Institute for Quantum Computing, University of Waterloo, Waterloo, Ontario N2L 3G1, Canada. [7]Department of Physics and Astronomy, Macquarie University, NSW 2109, Australia. [8]School of Mathematics and Physics, University of Queensland, Brisbane, QLD 4072, Australia. [9]Centre for Quantum Dynamics and Centre for Quantum Computation and Communication Technology, Griffith University, Brisbane, QLD 4111, Australia.

*To whom correspondence should be addressed. E-mail: h.wiseman@griffith.edu.au (H.W.); akiraf@ap.t.u-tokyo.ac.jp (A.F.)

Recall that $\overline{R}_{sq}$ (Eq. 2) is a function of σ_f^2, so the above expression for σ_s^2 is still implicit. The full solutions are given in (*26*), but in the parameter regime of our experiment, σ_s^2 is roughly proportional to $\sqrt{\overline{R}_{sq}}$. That is, by using a nonclassical beam with effective squeezing $\overline{R}_{sq} < 1$ we expect to be able to overcome the coherent-state limit (CSL) by a factor of $\sqrt{\overline{R}_{sq}}$.

Our experiment (Fig. 1C) used an 860-nm continuous-wave titanium sapphire laser. The phase-squeezed beam was added by an optical parametric oscillator (OPO). The OPO was driven below threshold by a 430-nm pump beam, generated by a second-harmonic-generation cavity. We obtained up to −4 dB of phase squeezing. The signal $\varphi(t)$ was produced by a digital random signal generator and a low-pass filter with a cutoff frequency of $\lambda/2\pi$. This was imposed on the phase-squeezed beam by using an electrooptic modulator. Homodyne detection was performed on this phase-modulated beam with an overall efficiency of $\eta = 0.85$. The homodyne current went to the optimal feedback filter [another low-pass filter with a cutoff frequency $\lambda/2\pi$ (*26*)]. Its output, $\varphi_f(t)$, was then shifted by $\pi/2$ and applied on the phase of the LO beam with another electrooptic modulator.

We recorded $\varphi(t)$, $I(t)$, and $\varphi_f(t)$ by an oscilloscope with a sampling rate of 100 MHz. Figure 2 shows a typical segment of the recorded signals, plus the smoothed estimate $\varphi_s(t)$. The parameters here are $\kappa = 1.9 \times 10^4 \pm 0.1 \times 10^4$ rad/s, $\lambda = 5.9 \times 10^4 \pm 0.5 \times 10^4$ rad/s, $|\alpha|^2 = 1.00 \times 10^6 \pm 0.06 \times 10^6$ s^{-1}, squeezing −3.1 ± 0.1 dB ($r_m = 0.36 \pm 0.01$) and antisqueezing 5.1 ± 0.1 dB ($r_p = 0.59 \pm 0.01$), from a pump beam power of 80 mW. The uncertainties represent 1 standard deviation. κ and λ are fixed through this paper. The current $I(t)$ has zero mean because the feedback loop is designed to operate the homodyne measurement at this point of maximum sensitivity (Fig. 1B). Although the filtered estimate $\varphi_f(t)$ has a visible delay because of its causal nature, the smoothed estimate $\varphi_s(t)$ does not, and the signal phase $\varphi(t)$ is reliably tracked.

To investigate the squeezing enhancement, we performed phase tracking with a fixed square amplitude $|\alpha|^2 = 1.00 \times 10^6 \pm 0.06 \times 10^6$ s^{-1} but with varying squeezing levels arising from OPO pump beam powers of 0, 30, 80, and 180 mW. Independently of the phase estimation, squeezing and antisqueezing levels were measured for each pump beam power (*26*). The red crosses in Fig. 3 show the MSEs of the smoothed estimates σ_s^2 as a function of the squeezing level. The MSE was calculated from 2 ms of data (2×10^5 samples). Repeating this 15 times gave the average MSE and its standard deviation.

Figure 3 shows three key results. First, the squeezing enhancement is verified: The MSEs are reduced below the CSL (i) by using phase-squeezed beams. Second, the experimental results are in good agreement with the prediction (ii) and in disagreement with the theory curve (iii), which is based on approximating the homodyne output current $I(t)$ to only first order in $[\varphi(t) - \varphi_f(t)]$ so that $\overline{R}_{sq} = e^{2r_m}$. Third, at the higher squeezing level the MSE is saturated, indicating the existence of an optimal squeezing level. Even in the theoretical curve (iv), for pure squeezed beams and zero loss, the MSE has a minimum. This curve corresponds to the fundamental limit imposed by Heisenberg's uncertainty principle for the phase and amplitude quadratures, namely $e^{-2r_p} \times e^{2r_m} \geq 1$. Although more squeezing decreases the e^{-2r_m} term in $\overline{R}_{sq}$, it increases the e^{2r_p} term because the tracking is imperfect, which itself is a consequence of the noise in the photocurrent (Eq. 2). This defines (self-consistently) the optimal degree of squeezing, which depends on the parameters $|\alpha|$, κ, and λ (*26*).

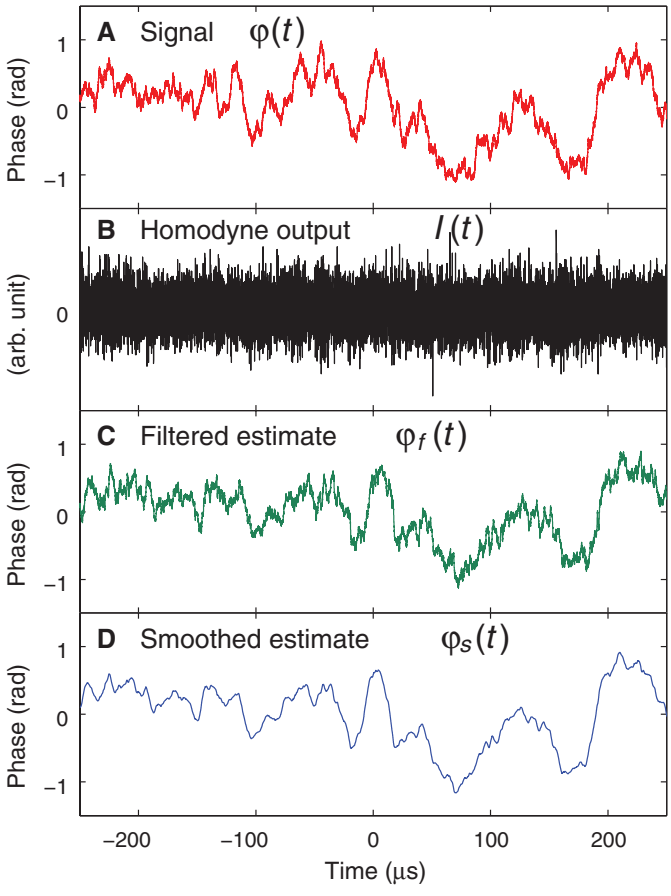

Fig. 2. Time domain results of phase estimate. (**A**) Signal phase to be estimated $\varphi(t)$. (**B**) Homodyne output current $I(t)$. (**C**) Filtered estimate $\varphi_f(t)$. (**D**) Smoothed estimate $\varphi_s(t)$.

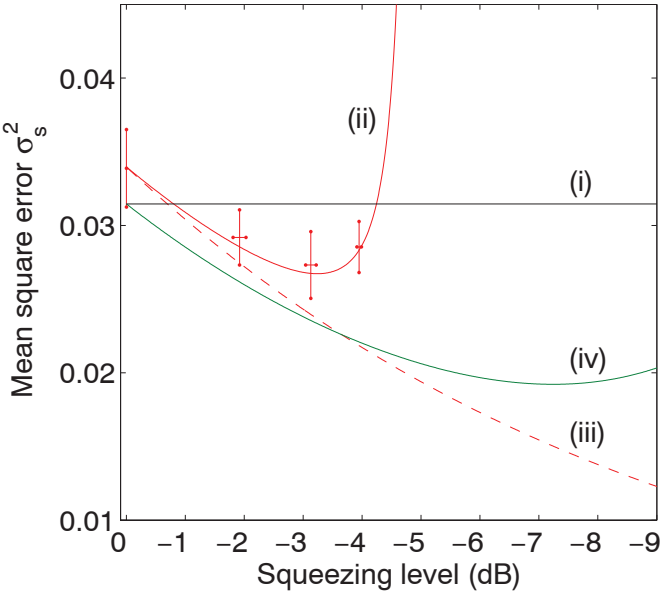

Fig. 3. Smoothed MSE σ_s^2 versus squeezing level. Red crosses represent experimental data. Trace (i) is the coherent-state limit, which is reachable with a coherent beam only if we have unit-detection efficiency $\eta = 1$. Trace (ii) is the theoretical curve from Eq. 3. Trace (iii) is the theoretical curve based on approximating the homodyne output current $I(t)$ to only first order in $[\varphi(t) - \varphi_f(t)]$ so that $\overline{R}_{sq} = e^{-2r_m}$. Trace (iv) is the theoretical curve from Eq. 3 for pure squeezed beams (i.e., without loss).

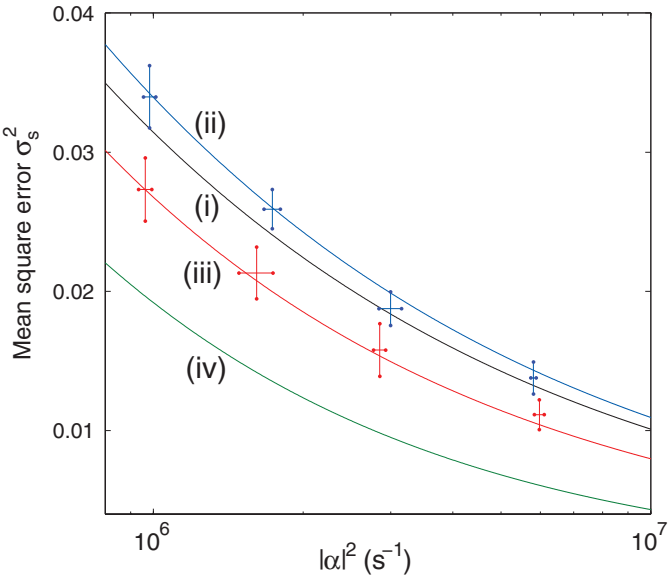

Fig. 4. Dependence of the smoothed MSE σ_s^2 on the amplitude squared $|\alpha|^2$. Blue and red crosses are experimental data for coherent and squeezed beams, respectively. Trace (i) is the coherent-state limit. Trace (ii) is the theoretical curve for coherent beams with the experimental setup (i.e., including inefficiency). Trace (iii) is the theoretical curve for squeezed beams, including inefficiency. Trace (iv) is the theoretical curve for pure squeezed beams and 100% efficiency, with the squeezing level optimized for each $|\alpha|^2$.

Experimentally, we varied the amplitude $|\alpha|$ while fixing the pump beam power to 80 mW, giving squeezing and antisqueezing levels of -3.2 ± 0.2 dB and 4.9 ± 0.3 dB, respectively. Theoretically, the optimal squeezing level increases with $|\alpha|$, and so too does the squeezing enhancement, without limit. However, for our experimental conditions ($10^6\ s^{-1} \leq |\alpha|^2 < 10^7\ s^{-1}$) the effect of keeping the squeezing fixed is minor (less than 3% difference to σ_s^2). Figure 4 shows the dependence of the MSE σ_s^2 on $|\alpha|$. The theoretical curves show good agreement with experiments. Over the whole amplitude range, the estimates with the squeezed beams surpass what is possible with coherent states, with σ_s^2, averaged over the four different amplitudes, being $15 \pm 4\%$ below the CSL. The conclusion is essentially unaltered if one calculates the CSL not in terms of $|\alpha|^2$ but in terms of the effective photon flux $\mathcal{N}_{\text{eff}}$, which equals $|\alpha|^2$ plus the extra photons resulting from the squeezed vacuum fluctuations in the relevant spectral range (*26*).

We have tracked the phase of a squeezed optical field that varies stochastically in time over a substantial angular range. Our use of Kalman filtering in real-time adaptive measurements of nonclassical systems could be applied also in solid-state and nanomechanical devices. Optimizing both the degree of squeezing and its bandwidth according to the experimental conditions would allow a completely rigorous treatment of photon flux. Lower losses and more squeezing would then enable a dramatic improvement to a precision that scales differently with photon flux, with $\sigma^2 \propto \mathcal{N}^{-5/8}$ (*20*) as opposed to the $\sigma^2 \propto \mathcal{N}^{-1/2}$ in the current setup.

References and Notes

1. R. Slavík *et al.*, *Nat. Photonics* **4**, 690 (2010).
2. J. Chen, J. L. Habif, Z. Dutton, R. Lazarus, S. Guha, *Nat. Photonics* **6**, 374 (2012).
3. V. Giovannetti, S. Lloyd, L. Maccone, *Nat. Photonics* **5**, 222 (2011).
4. C. W. Helstrom, *Quantum Detection and Estimation Theory* (Academic Press, New York, 1976).
5. V. Giovannetti, S. Lloyd, L. Maccone, *Science* **306**, 1330 (2004).
6. H. M. Wiseman, G. J. Milburn, *Quantum Measurement and Control* (Cambridge University Press, Cambridge, 2010).
7. C. M. Caves, *Phys. Rev. D Part. Fields* **23**, 1693 (1981).
8. K. Goda *et al.*, *Nat. Phys.* **4**, 472 (2008).
9. J. Abadie *et al.*, *Nat. Phys.* **7**, 962 (2011).
10. K. Inoue, E. Waks, Y. Yamamoto, *Phys. Rev. Lett.* **89**, 037902 (2002).
11. G. Y. Xiang, B. L. Higgins, D. W. Berry, H. M. Wiseman, G. J. Pryde, *Nat. Photonics* **5**, 43 (2011).
12. T. Nagata, R. Okamoto, J. L. O'Brien, K. Sasaki, S. Takeuchi, *Science* **316**, 726 (2007).
13. H. M. Wiseman, *Phys. Rev. Lett.* **75**, 4587 (1995).
14. H. M. Wiseman, R. B. Killip, *Phys. Rev. A* **57**, 2169 (1998).
15. D. W. Berry, H. M. Wiseman, *Phys. Rev. Lett.* **85**, 5098 (2000).
16. M. A. Armen, J. K. Au, J. K. Stockton, A. C. Doherty, H. Mabuchi, *Phys. Rev. Lett.* **89**, 133602 (2002).
17. B. L. Higgins, D. W. Berry, S. D. Bartlett, H. M. Wiseman, G. J. Pryde, *Nature* **450**, 393 (2007).
18. A. Hentschel, B. C. Sanders, *Phys. Rev. Lett.* **104**, 063603 (2010).
19. D. W. Berry, H. M. Wiseman, *Phys. Rev. A* **65**, 043803 (2002).
20. D. W. Berry, H. M. Wiseman, *Phys. Rev. A* **73**, 063824 (2006).
21. T. A. Wheatley *et al.*, *Phys. Rev. Lett.* **104**, 093601 (2010).
22. M. Tsang, J. H. Shapiro, S. Lloyd, *Phys. Rev. A* **79**, 053843 (2009).
23. M. Tsang, H. M. Wiseman, C. M. Caves, *Phys. Rev. Lett.* **106**, 090401 (2011).
24. M. Tsang, *Phys. Rev. Lett.* **102**, 250403 (2009).
25. C. W. Gardiner, *Handbook of Stochastic Methods* (Springer, Berlin, 1985).
26. See supplementary materials on *Science* Online.

Acknowledgments: This work was partly supported by Project for Developing Innovation Systems, Grants-in-Aid for Scientific Research, Global Center of Excellence, Advanced Photon Science Alliance, Funding Program for World-Leading Innovative R&D on Science and Technology commissioned by the Ministry of Education, Culture, Sports, Science and Technology (MEXT) of Japan, Strategic Information and Communications R and D Promotion program of the Ministry of Internal Affairs and Communications of Japan, and the Australian Research Council projects CE110001029, DP1094650, and FT100100761.

Supplementary Materials

www.sciencemag.org/cgi/content/full/337/6101/1514/DC1
Materials and Methods
Supplementary Text
Figs. S1 to S8
References (*27–30*)

28 May 2012; accepted 13 August 2012
10.1126/science.1225258

Subtractive Patterning via Chemical Lift-Off Lithography

Wei-Ssu Liao,[1,2] Sarawut Cheunkar,[1,3] Huan H. Cao,[1,2] Heidi R. Bednar,[1,2] Paul S. Weiss,[1,2,3,4,5]* Anne M. Andrews[1,2,6,7]*

Conventional soft-lithography methods involving the transfer of molecular "inks" from polymeric stamps to substrates often encounter micrometer-scale resolution limits due to diffusion of the transferred molecules during printing. We report a "subtractive" stamping process in which silicone rubber stamps, activated by oxygen plasma, selectively remove hydroxyl-terminated alkanethiols from self-assembled monolayers (SAMs) on gold surfaces with high pattern fidelity. The covalent interactions formed at the stamp-substrate interface are sufficiently strong to remove not only alkanethiol molecules but also gold atoms from the substrate. A variety of high-resolution patterned features were fabricated, and stamps were cleaned and reused many times without feature deterioration. The remaining SAM acted as a resist for etching exposed gold features. Monolayer backfilling into the lift-off areas enabled patterned protein capture, and 40-nanometer chemical patterns were achieved.

High-throughput molecular printing strategies with high feature resolution are central goals for lithography. However, progress has been impeded by the conflicting aims of large-area fabrication versus precision, and of convenience versus cost (*1–4*). For instance, although photolithography enables patterning over large areas (centimeters), the prototyping process is time-consuming and resolution is restricted by light diffraction (*1–3*). Patterning by electron beam lithography (EBL) or scanning probe lithography (SPL) techniques, such as dip-pen nanolithography,